THE JOURNAL OF PHYSICAL CHEMISTRY C
A JOURNAL OF THE AMERICAN CHEMICAL SOCIETY

pubs.acs.org/JPCC

Article

First-Principles Study of Bonding-Driven Selectivity in CO_2 Electroreduction on Metal−Nitrogen−Carbon Catalysts

Meixu Lu, Lin Tao,* Yaqiong Su,* Yimeng Sun, Davoud Dastan, Javed Rehman, Han Zhang, Hongwei Zhao, Lixiang Li, and Baigang An*

Cite This: https://doi.org/10.1021/acs.jpcc.5c07261

Read Online

ACCESS | Metrics & More | Article Recommendations | Supporting Information

ABSTRACT: Single-atom catalysts (SACs) have emerged as promising candidates for the carbon dioxide reduction reaction (CO_2RR), and the design of new SACs is of great significance. This study introduces a series of transition metal SACs anchored on nitrogen-doped single-layer graphene (denoted as TM-C_2N, with TM representing Fe, Ni, Cu, Pd, Ag, and Sn), designed for the selective conversion of CO_2 to CO or formic acid. Utilizing first-principles computational approaches, the structural integrity, CO_2 adsorption, and activation dynamics of these catalysts have been systematically investigated. Our findings reveal that the TM-C_2N catalysts not only manifest exceptional structural stability but also exhibit superior CO_2 adsorption and activation capabilities, coupled with an effective suppression of the competing hydrogen evolution reaction (HER). Gibbs free energy analyses have delineated distinct reaction pathways leading to HCOOH and CO formation on TM-C_2N. Notably, Ni-C_2N stands out as the most active catalysts, as evidenced by their favorable limiting potentials. The role of bonding interactions in elucidating the gas−solid interface adsorption mechanism is also highlighted. These insights offer valuable theoretical guidance for the fine-tuning of C_2N-based catalysts in experimental settings and have broad implications for the development of efficient transition metal SACs for CO_2 reduction.

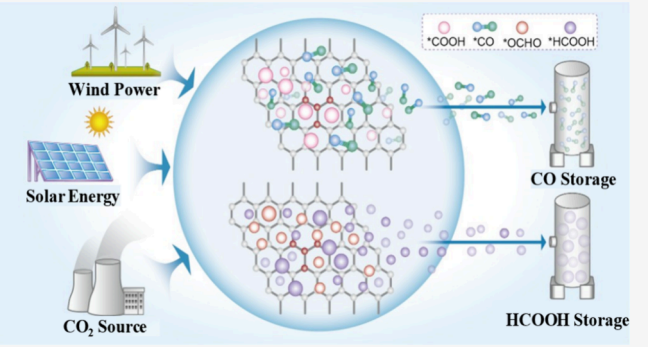

INTRODUCTION

With the development of industry and economy, more and more fossil fuels have been consumed, and the continuous intensification of CO_2 emissions has led to abnormal changes in global climate and a general warming trend.[1] Therefore, how to reduce the impact of excessive CO_2 on human production and life has become a major issue. Although CO_2 is a greenhouse gas, a large number of high concentrations of CO_2 can also be regarded as a rich carbon source, so the efficient conversion and effective use of CO_2 has become a crucial step to solve the greenhouse effect and achieve carbon neutrality.[2−4] CO_2 can be chemically transformed into valuable products such as methanol, methane, and formic acid through catalytic methods like hydrogenation and advanced conversion technologies. Formic acid, specifically, is extensively utilized as a feedstock in chemical manufacturing, pharmaceutical synthesis, and food processing industries. Recent advancements in CO_2 conversion have introduced more efficient and sustainable approaches, paving the way for broader industrial applications. Among them, the electrochemical reduction of CO_2 has become a particularly effective method of CO_2 conversion.[5−9]

Nevertheless, the high overpotential associated with the catalysts, as well as the inherent thermodynamic stability of CO_2 and the increased activation energy barrier, hinders the wider application of CO_2RR.[10−12] Moreover, HER often supersedes CO_2RR as a side reaction due to its relatively lower overpotential, further complicating the process. It is, therefore, imperative to design and develop efficient electrocatalysts that can diminish the overpotential required for CO_2 reduction, a pursuit of significant scientific and technological importance.[13,14]

Among various catalytic materials, single-atom catalysts (SACs) have attracted widespread attention due to their exceptional catalytic activity and remarkable atomic efficiency. SACs were first synthesized in 2011 and have demonstrated outstanding catalytic performance in the reduction of CO_2.[15,16] Designing and synthesizing more efficient metal single-atom catalysts is both scientifically and practically significant. Substrate materials with large surface areas and excellent electronic and thermal properties, such as metal oxides, 2D materials, graphene, hexagonal boron nitride, and 2D polymer

Received: October 22, 2025
Revised: December 18, 2025
Accepted: December 19, 2025

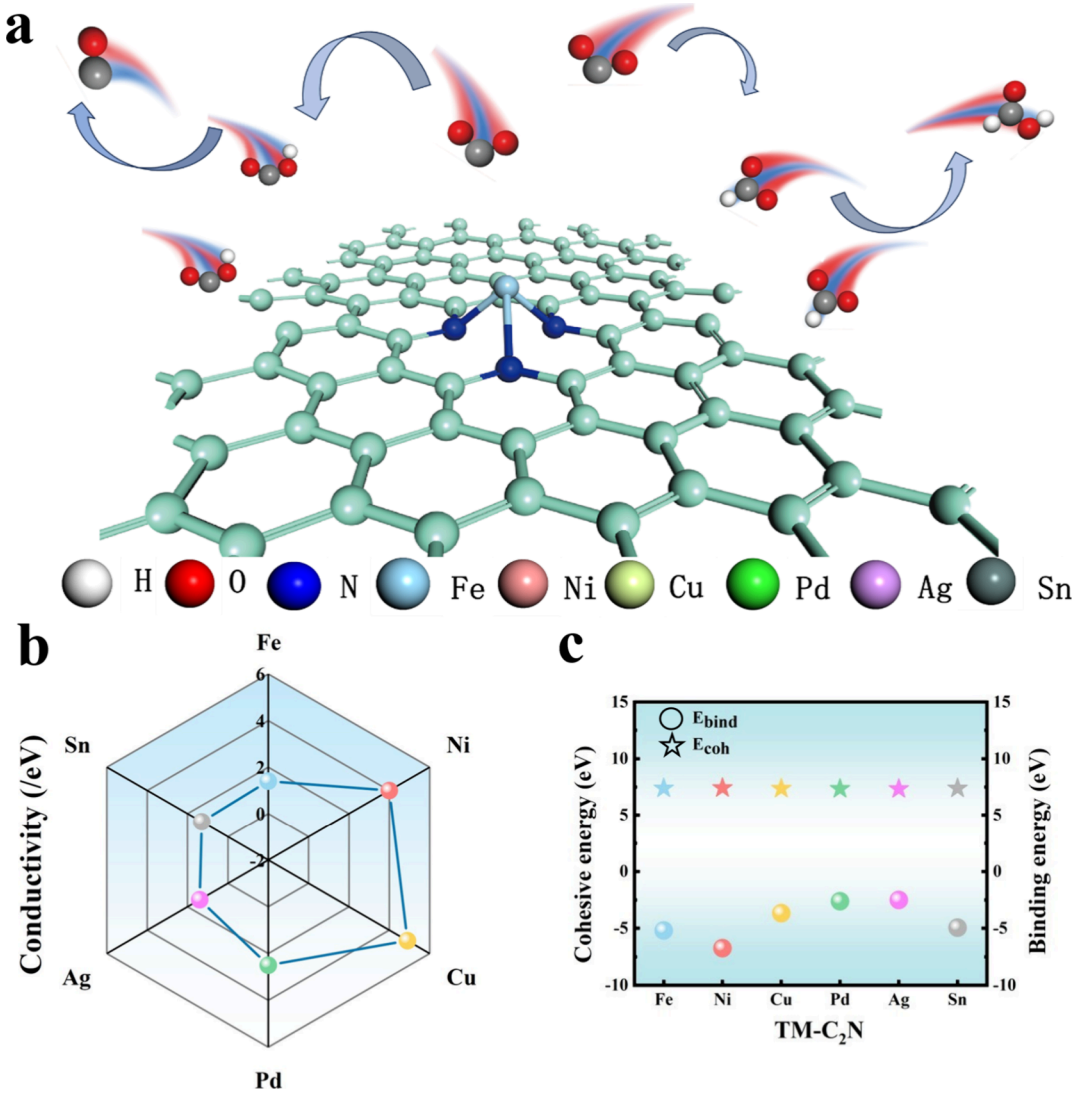

Figure 1. (a) Enhanced CO_2 conversion with tuned transition metal-loaded C_2N. (b) Conductivity of different catalyst materials based on the height of the DOS curve at the Fermi level. (c) Cohesive energy and binding energy of TM-C_2N structures.

metal phthalocyanine sheets, have been employed as catalysts carriers.[17−19] Recently, a novel two-dimensional material C_2N monolayer with high structural and thermal stability has been discovered. The special structural composition can provide the best metal impurity site and significantly improve the catalysts performance.[20−23]

A deep understanding of the underlying mechanisms governing the electrocatalytic reduction of CO_2 is critical for the rational design and optimization of catalysts. Extensive research has been conducted to explore the potential mechanisms of CO_2RR, with a specific focus on the use of density functional theory (DFT) calculations to provide a robust quantum chemical framework.[24−26] Advances in nanotechnology have enabled the fine-tuning of catalysts structures at the nanoscale, thereby enhancing stability, catalytic activity, and product selectivity.[27,28] Notably, SACs, double-atom catalysts (DACs), and triple-atom catalysts (TACs), characterized by their highly dispersed active sites, have demonstrated low overpotentials, elevated conversion efficiencies, and commendable product selectivity, along with an inherent capacity to suppress the hydrogen evolution reaction, which augurs well for their broad application prospects.[29−32]

Prior research has established that SACs and DACs, when modified with metal atoms such as Cu, Pd, Ag, and Pt, exhibit superior CO_2RR catalytic activity.[33−37] Research has explored the use of copper-doped nickel metal as a catalytic substrate for the CO_2 reduction reaction.[38] Building on this, a nitrogen/sulfur-coordinated iron−nickel dual-atom catalyst was developed.[39] Separate studies have shown that "vacancies" and nitrogen doping in graphene can effectively stabilize iron atom catalysts.[40] Concurrently, a single-atom tin catalyst based on SnS_2 material was found to efficiently convert CO_2 to formic acid.[41] Additionally, research indicates that incorporating hydrogen into copper single-atom catalysts can modulate their microstructure.[42] While single-metal sites have been confirmed to possess significant potential for CO_2 conversion, most existing research has been limited to individual metals and specific products. In contrast, this study systematically compares the performance of a series of single-atom catalysts in the electrochemical CO_2 reduction reaction, aiming to reveal the decisive role of the intrinsic properties of metals in determining catalytic pathways. Selecting appropriate catalysts

https://doi.org/10.1021/acs.jpcc.5c07261
J. Phys. Chem. C XXXX, XXX, XXX−XXX

materials can effectively curtail the aggregation of transition metal single atoms, simplifying the synthesis process and bolstering catalyst stability through augmented interfacial interactions.[43] Nitrogen-doped graphene (C_2N), widely utilized as a support material for SACs, holds significant application potential owing to its periodic uniformity and elevated thermal stability.[44−48] However, given the exorbitant costs and scarcity associated with noble metals, there is an imperative to develop cost-effective, high-performance catalysts as viable alternatives.

In this study, the present investigation systematically assesses the catalytic efficacy of metal single-atom materials anchored on nitrogen-doped graphene (denoted as TM-C_2N, with TM representing Fe, Ni, Cu, Pd, Ag, and Sn), employing first-principles computational methodologies. Initially, the stability and electronic configuration of the TM-C_2N catalysts are ascertained through cohesive energy calculations. Subsequently, leveraging d-band center theory and a comprehensive electronic structure analysis, the adsorption energy and activation propensity of CO_2 are elucidated. Ultimately, through an analysis of the Gibbs free energy profiles, the optimal reaction pathways for the formation of various products, alongside their corresponding limiting and overpotentials, are delineated, thereby shedding light on the underlying mechanisms governing the CO_2 reduction process.

EXPERIMENTAL SECTION

The computational work was performed using the Dmol^3 software, which is based on density functional theory under periodic boundary conditions.[49,50] The elements involved include carbon, nitrogen, oxygen, hydrogen, copper, iron, palladium, tin, silver, and nickel, with their valence electron configurations being $2s^22p^2$, $2s^22p^3$, $2s^22p^4$, $1s^1$, $3d^{10}4s^1$, $3d^64s^2$, $4d^{10}$, $5s^25p^2$, $4d^{10}5s^1$, and $3d^84s^2$, respectively. The interaction between valence and core electrons was described using the projector augmented wave (PAW) method. The exchange-correlation effects were simulated using the Perdew−Burke−Ernzerhof (PBE) functional within the generalized gradient approximation (GGA) framework.[51] To improve the precision of the total energy calculations, spin polarization was incorporated, and a dispersion correction (Grimme D2) was implemented.[52,53] For structural optimization and electronic property calculations, strict convergence criteria were adopted: The convergence threshold for total energy was set to 10^{-5} eV, and the convergence threshold for atomic forces was 0.01 eV/Å. A Γ-point-centered *k*-point mesh with a 3 × 3 × 1 grid was employed for Brillouin zone sampling, which balances computational efficiency and accuracy for 2D monolayer systems by sufficiently covering the electronic states near the Fermi level. To eliminate spurious interactions between adjacent periodic supercells, a vacuum layer of 20 Å was introduced vertically to the TM-C_2N monolayer plane; this thickness is greater than the typical van der Waals interaction range (≈5−10 Å), ensuring no artificial coupling between periodic images. An implicit solvation model was employed to represent the solvent, with the dielectric constant set to 78.4 for water.[54]

RESULTS AND DISCUSSION

Stability of TM-C_2N Catalysts

The single-atom catalyst model is constructed on a 2 × 2 supercell of the C_2N lattice. The metal single atoms are positioned atop the C_2N lattice, each metal atom covalently bonded to three nitrogen atoms (Figure S1). To elucidate the conductivity and stable configuration of the C_2N catalysts for CO_2RR modified by six distinct metals, a schematic representation is provided in Figure 1a. The catalysts can be used as a good transfer material, and its electrical conductivity is one of the most important indicators. The density of states (DOS) curve height at the Fermi level for TM-C_2N was calculated, serving as a pivotal parameter for assessing catalyst conductivity.[55−59] In Figure 1b, the electrical conductivity of all metal-doped monolayers is enhanced, which indicates that the method of metal atomic modification is suitable for improving the performance of the catalysts. It is worth noting that the increase in conductivity of the monolayer materials doped with Cu and Ni atoms is the most significant.

Given that stability is a fundamental requirement for catalyst applications, the stability of the TM-C_2N catalysts is gauged through cohesive energy calculations and the binding energies of the metal atoms.[60−62] The detailed calculation of cohesive energy can be found in the Supporting Information. As shown in Figure 1c, the cohesive energies of the TM-C_2N catalysts are ranked in the order of Fe-C_2N, Ni-C_2N, Cu-C_2N, Pd-C_2N, Ag-C_2N, and Sn-C_2N, with Ni-C_2N exhibiting the highest stability. The cohesive energies of the TM-C_2N catalysts surpass those of carbides (4.12−6.45 eV/atom)[63] and silicene (5.16 eV/atom),[64] underscoring their superior stability. To assess the thermodynamic stability of TM-C_2N structures, we performed ab initio molecular dynamics (AIMD) simulations. The simulations were conducted at 500 K for 10 ps, with structural snapshots recorded every 1 fs. As illustrated in Figures S2 and S3, the results demonstrate that TM-C_2N materials maintain structural integrity under these conditions, highlighting their inherent stability.

Furthermore, leveraging the formation environment of single atoms on the nitrogen−carbon carrier, the binding energies at the interface between the carrier site and metal atoms are harnessed to evaluate the stability of the single-atom catalysts. The results indicate that these binding energies possess relatively high magnitudes, thereby ensuring the stability of the catalysts. To assess the stability of electrocatalysts during long-term operation under reaction conditions, the dissolution potential is computed.

To enhance our comprehension of the interactions between metal single atoms and C_2N, computational analyses of DOS, PDOS, and charge density at the interface for TM-C_2N catalysts were conducted. As depicted in Figures S5−S7, in the vicinity of the Fermi level, a pronounced overlap of electronic wave function is observed between the d orbitals of the metal single atoms and the p orbitals of nitrogen within the C_2N lattice, signifying interactions at the atomic level. Notably, in the cases of Cu-C_2N and Ni-C_2N, an increased number of overlapping peaks are evident, suggesting a more pronounced interaction between the Cu and Ni atoms and the nitrogen atoms when compared to other metals studied. This observation is instrumental in explaining the enhanced stability of the Cu-C_2N and Ni-C_2N catalysts. Furthermore, the charge density analysis discloses considerable electron accumulation and delocalization at the interface of metal atoms and the substrate, substantiating the existence of interactions. These interactions culminate in augmented bonding energies and diminished bond lengths between the Cu and Ni atoms and the nitrogen atoms.

https://doi.org/10.1021/acs.jpcc.5c07261
J. Phys. Chem. C XXXX, XXX, XXX−XXX

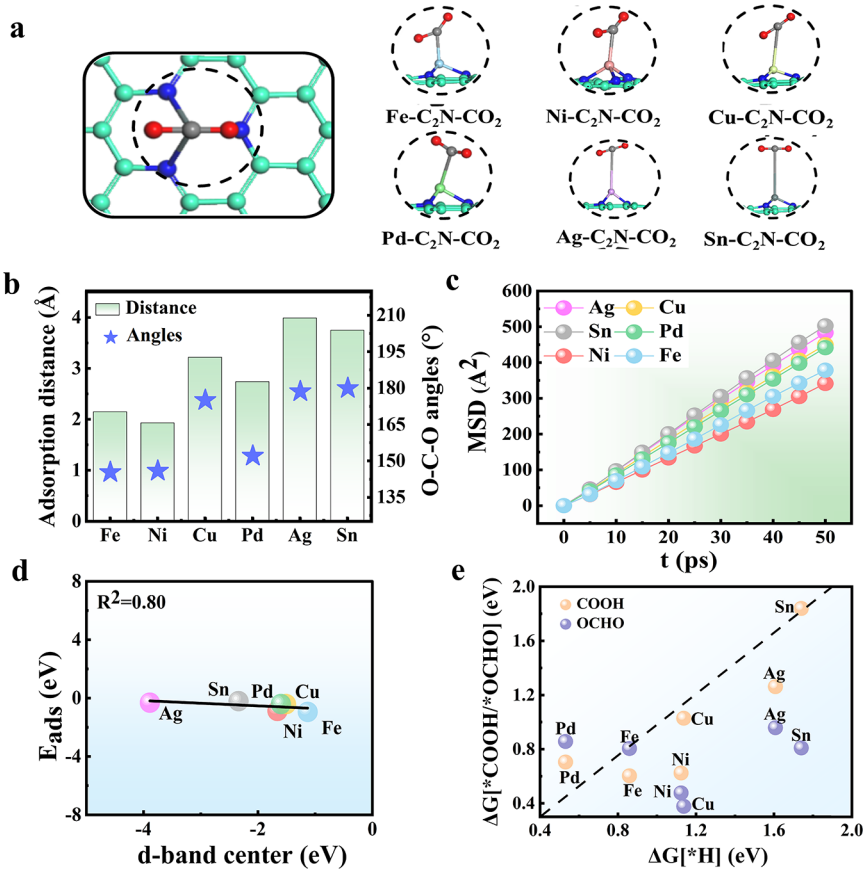

Figure 2. (a) Optimal structures of CO_2 on the TM-C_2N catalysts. (b) Activated C−M bond length and O−C−O bond angle bending. (c) Diffusion behaviors of CO_2 on TM-C_2N. (d) Linear relationship between the d-band center of TM-C_2N and the adsorption energy of CO_2. (e) Free energy change of the first hydrogenation steps in CO_2RR vs HER.

Activation and Selectivity

Stable CO_2 adsorption is a key prerequisite for the efficient operation of CO_2RR. The extent of CO_2 activation is indicative of the catalysts' performance to a certain degree. As depicted in Figure 2a, CO_2 molecules stably adsorb onto the catalyst surface, with significant alterations in molecular configuration, signifying effective initial activation (Figure S8). The results indicate in Figure 2b that after the adsorption of CO_2 on the surface, there is a significant change in the C−M bond length (when CO_2 is bonded to the surface) within the range from 1.88 to 3.50 Å. Meanwhile, the O−C−O bond angle also shows a bending from 145.3 to 179.4°. These remarkable changes in the structural parameters fully confirm the effective activation of the CO_2 molecule. Additionally, our detailed analysis of the DOS curves between gas molecules and catalyst surface active sites reveals significant interactions for Cu and Ni with CO_2, generating distinct new energy peaks (Figures S9 and S10). Notably, the hybridization between metal d orbitals and nonmetal p orbitals is the predominant factor.

The diffusion characteristics of CO_2 on the catalyst surface are determinants of the reaction rate. To assess the practical application performance of these catalysts, molecular dynamics simulations were employed to calculate the diffusion coefficients of CO_2 across various material surfaces, thereby characterizing their diffusion properties. To study the diffusion behavior of CO_2 on the TM-C_2N surface, we performed molecular dynamics (MD) simulations. The detailed calculation can be found in the Supporting Information and Figures S11 and S12. Ni-C_2N exhibits excellent CO_2 adsorption capacity, which is attributed to its low diffusion kinetic characteristics. Meanwhile, CO_2 molecules do not exhibit stable adsorption on the uppermost surface and show a preferential distribution throughout the bulk phase. Initially, the MSD for the TM-C_2N catalysts was calculated and is presented in Figure 2c. The results indicate that Ni-C_2N has good diffusion performance, as inferred from the slope of the MSD plot. Furthermore, the diffusion coefficient, which impacts the surface diffusion of CO_2, can be derived from Einstein's equation for diffusion. The diffusion coefficients of CO_2 are 1.66 for Fe-C_2N, 1.16 for Ni-C_2N, 1.46 for Cu-C_2N, 1.47 for Pd-C_2N, 1.56 for Ag-C_2N, and 1.28 for Sn-C_2N. The magnitude of the diffusion coefficient directly influences CO_2 surface diffusion. More stable CO_2 adsorption and enhanced catalytic efficacy are correlated with a smaller coefficient.

To further elucidate the adsorption behavior of CO_2 on the catalysts, calculations of the d-band center for the metal single-atom catalysts were performed. Adsorption energy is specified as $E_{ads} = E_{total} - (E_{monolayer} + E_{gas})$, where E_{ads} represents the adsorption energy (eV), E_{total} is the total energy, $E_{monolayer}$ is the energy of the two-dimensional monolayer, and E_{gas} is the energy of the gas (eV). Figure 2d delineates the correlation between the d-band center of the metal single atoms and the CO_2 adsorption energy. The d-band center shows a significant correlation with catalytic activity (R^2 = 0.80). This aligns with the predictive trend of the d-band center theory, which states that a moderate d-band center enables the formation of an optimal binding energy between the catalysts and reactants,

https://doi.org/10.1021/acs.jpcc.5c07261
J. Phys. Chem. C XXXX, XXX, XXX−XXX

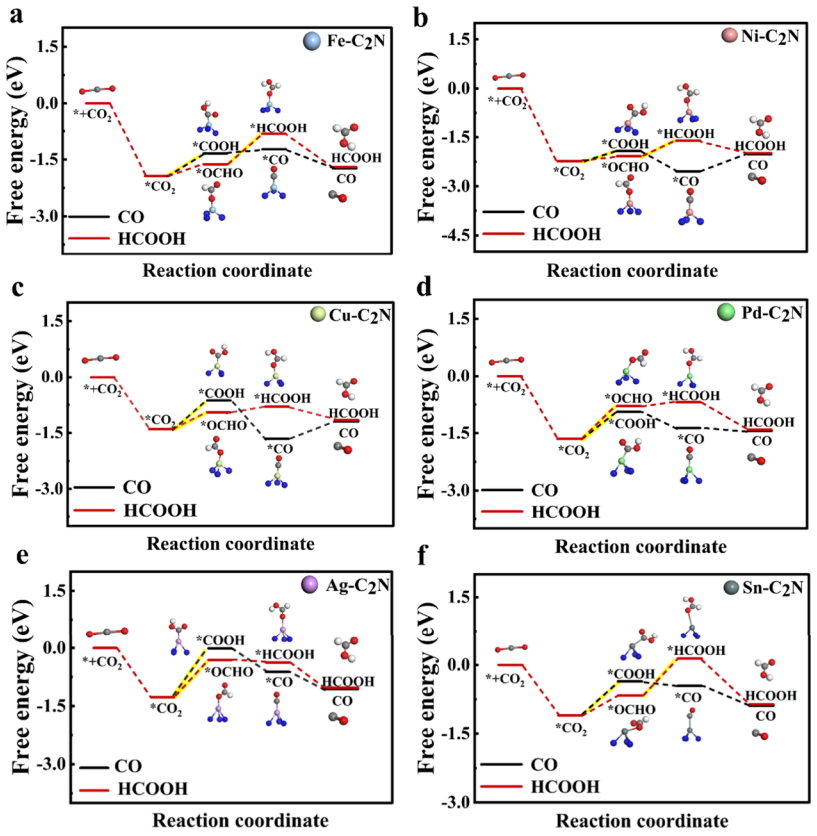

Figure 3. Gibbs free energy distribution diagram of the CO_2 reduction pathway. (a) Fe-C_2N, (b) Ni-C_2N, (c) Cu-C_2N, (d) Pd-C_2N, (e) Ag-C_2N, and (f) Sn-C_2N.

thereby enhancing catalytic efficiency. From an electronic structure perspective, such moderate binding energy typically corresponds to lower electron occupancy in the reactant-catalyst antibonding orbitals, avoiding the weakening of binding caused by excessive occupation of antibonding states. From a kinetic perspective, the propensity for the HER to occur as a side process can significantly hinder the advancement of the electrocatalytic reduction of CO_2. Consequently, it is imperative for efficient catalysts to effectively suppress the HER. The Gibbs free energies of hydrogen adsorption on the surfaces of Fe-C_2N, Ni-C_2N, Cu-C_2N, Pd-C_2N, Ag-C_2N, and Sn-C_2N, catalysts was determined to be 0.85, 1.12, 1.13, 0.53, 1.60, and 1.74 eV, respectively. When compared with the Gibbs free energy of CO_2 adsorption (Table S1), CO_2 adsorption is energetically more favorable than hydrogen adsorption in this reaction system. These findings offer reliable data and a robust theoretical foundation for elucidating the suppression of the HER.

The results further clarify the intrinsic reason for the effective suppression of the HER by TM-C_2N, the synergistic effect of thermodynamic preference and electronic structure regulation. Thermodynamically, the positive Gibbs free energy of H^+ adsorption stands in stark contrast to the negative adsorption energy of CO_2, enabling CO_2 to competitively occupy the active TM sites and reduce the chance of H^+ binding, which directly hinders the initial step of HER. Electronically, charge density and PDOS analyses confirm that the d orbitals of TM atoms form strong hybridization with the p orbitals of N atoms in C_2N. This orbital interaction redirects the electron density of active sites to interact with the O 2p orbitals of CO_2 rather than the 1s orbital of H^+, thereby weakening the binding strength between H and the catalyst surface.

Furthermore, based on the principles of adsorption energetics, it is apparent that CO_2 is more readily adsorbed onto the TM-C_2N catalyst surface compared to hydrogen, which effectively mitigates the onset of the HER. Additionally, during the initial protonation step of CO_2 hydrogenation, two key intermediates are produced: *COOH (via the reaction $*CO_2 + H^+ + e^- \rightarrow *COOH$) and *OCHO (via the reaction $*CO_2 + H^+ + e^- \rightarrow *OCHO$). Meanwhile, for the HER, the formation of the *H intermediate (via the reaction $* + H^+ + e^- \rightarrow *H$) is observed. As depicted in Figure 2e, when $\Delta G(*COOH)$ and $\Delta G(*OCHO)$ are less than $\Delta G(*H)$, the reaction requires less energy and is more conducive to product formation, upon comparison of the Gibbs free energy changes $\Delta G(*COOH)$ and $\Delta G(*OCHO)$ with $\Delta G(*H)$, the TM-C_2N catalysts are situated in the lower right region of the selectivity diagram, which is the CO_2RR selectivity advantage zone. A preference for the formation of *COOH or *OCHO intermediates is indicated by this structural positioning. Taking these findings into account, it is evident that TM-C_2N catalysts demonstrate a marked selectivity for CO_2RR, concurrently efficaciously suppressing the HER as a competing side reaction.

CO_2 Reduction Pathway

Figure 3 presents the adsorption configurations and the corresponding free energy landscapes for the intermediates produced during the CO_2 reduction process on TM-C_2N catalysts. CO_2 adsorption happens on its own without needing extra energy. A negative Gibbs free energy also gives an extra push from a thermodynamic point of view for the CO_2 reduction reaction to take place. This negative Gibbs free

https://doi.org/10.1021/acs.jpcc.5c07261
J. Phys. Chem. C XXXX, XXX, XXX−XXX

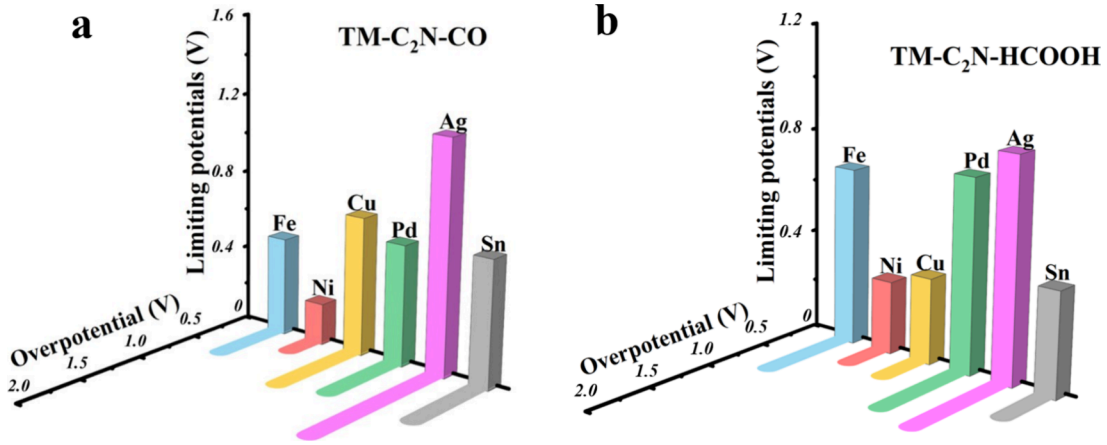

Figure 4. Limiting potential and overpotential of CO_2RR. (a) CO and (b) HCOOH.

energy helps key parts like *COOH and *CO form more easily after CO_2 gets adsorbed. As a result, the energy needed to start the reaction goes down, and the reaction speeds up. HCOOH is predominantly produced via the *OCHO intermediate, a pathway that entails the direct addition of H to CO_2, culminating in the formation of HCOOH. CO is primarily generated via the *COOH intermediate, which subsequently leads to the release of CO. The CO_2-to-CO conversion pathway on TM-C_2N catalysts is delineated as follows: $CO_2 \rightarrow *CO_2 \rightarrow *COOH \rightarrow *CO \rightarrow CO$, with the rate-determining step being the transformation of $*CO_2$ to *COOH. The maximum ΔG for the rate-limiting step are 0.61 eV for Fe-C_2N, 0.30 eV for Ni-C_2N, 0.80 eV for Cu-C_2N, 0.71 eV for Pd-C_2N, 1.27 eV for Ag-C_2N, and 0.74 eV for Sn-C_2N, respectively.

The pathway for CO_2 conversion to HCOOH on TM-C_2N catalysts is as follows: $CO_2 \rightarrow$ *OCHO $\rightarrow$ *HCOOH $\rightarrow$ HCOOH, with the rate-determining step identified as the initial $*CO_2$ to *OCHO conversion. Among them, the rate-determining step for Fe, Ni, and Sn is *OCHO to *HCOOH. The corresponding maximum ΔG changes for the rate-limiting step in the HCOOH formation pathway are 0.80 eV for Fe-C_2N, 0.40 eV for Ni-C_2N, 0.45 eV for Cu-C_2N, 0.86 eV for Pd-C_2N, 0.97 eV for Ag-C_2N, and 0.52 eV for Sn-C_2N. Among them, Ni shows the best advantages in the CO conversion path. Adsorption energy calculations for the *COOH and *OCHO intermediates on Ni-C_2N yield values of −2.44 and −2.35 eV, respectively. These results highlight the significant superiority of Ni-C_2N in activating intermediates, leading to a reduced free energy barrier for the reduction pathway.

Catalytic Performance

To quantitatively delineate catalyst performance, the limiting potential (U_L) and overpotential (η) were meticulously calculated and are hereby utilized as metrics of catalytic efficacy. Figure 4a presents the limiting potentials and overpotentials associated with the conversion of CO_2 to CO across a spectrum of catalysts, including Fe-C_2N, Ni-C_2N, Cu-C_2N, Pd-C_2N, Ag-C_2N, and Sn-C_2N. Overpotential, which is the difference between the limiting potential for product formation and the equilibrium potential, is a key indicator for assessing the performance of electrochemical systems. The theoretical equilibrium potentials for the reduction reactions yielding CO and HCOOH are established at 0.21 and 0.24 V, respectively. A near-zero U_L, as observed in Figure 4a, signifies a lower energetic barrier to produce the corresponding product. The U_L for CO production is ranked in ascending order as follows: Ni-C_2N, Fe-C_2N, Pd-C_2N, Cu-C_2N, Sn-C_2N, and Ag-C_2N. Similarly, the overpotentials required for CO generation are ordered from the lowest to the highest: Ni-C_2N, Fe-C_2N, Pd-C_2N, Cu-C_2N, Sn-C_2N, and Ag-C_2N. Considering both the limiting potential and overpotential, Ni-C_2N exhibits the best performance in CO production (Figure 4b). Consequently, the utilization of TM-C_2N catalysts in the context of CO_2RR is deemed viable. This study has thus explored the exceptional performance of TM-C_2N catalysts in the electrocatalytic reduction of CO_2, with Ni-C_2N surpassing the performance of the other five catalysts evaluated.

Catalytic Mechanism

In this section, the molecular orbital framework is explored to unravel the mechanisms underpinning the superior performance of Ni-C_2N catalysts, with a specific focus on the interactions between key intermediates and catalytically active sites. The role of bonding orbitals is critical in adsorption processes, where the initial interaction must be carefully balanced-neither too strong nor too weak. Therefore, crystal orbital Hamilton population (COHP) calculations were performed to analyze the key intermediates associated with the most effective transition metal catalysts (Figure 5a). Achieving an optimal balance in these interactions is essential for developing high-performance catalysts.

Figures S13 and S14 display the optimal adsorption geometries, charge density distributions, and DOS for *COOH and *OCHO on TM-C_2N catalysts. Notable charge redistribution is observed at the interaction sites between *COOH/*OCHO and TM-C_2N. The DOS analysis indicates significant orbital hybridization between nonmetal p orbitals and metal d orbitals, which enhances the desorption and reduction of CO and HCOOH on TM-C_2N catalysts. Therefore, these findings underscore the catalytic performance of TM-C_2N for the conversion of CO_2 to CO and HCOOH.

Figure 5b,c illustrates the bonding and antibonding regions at the Fermi level between the TM-C_2N surface and gas-phase atoms, with the corresponding ICOHP (Integrated Crystal Orbital Hamiltonian Population) values provided for clarity. The ICOHP was calculated to quantify the bond strength, with more negative values indicating stronger bonding. Detailed calculations are presented in Figure S15. A higher ICOHP value corresponds to stronger bond energy and greater energy required for desorption. The adsorption strength between a catalyst and reactant molecules should be maintained within an

https://doi.org/10.1021/acs.jpcc.5c07261
J. Phys. Chem. C XXXX, XXX, XXX−XXX

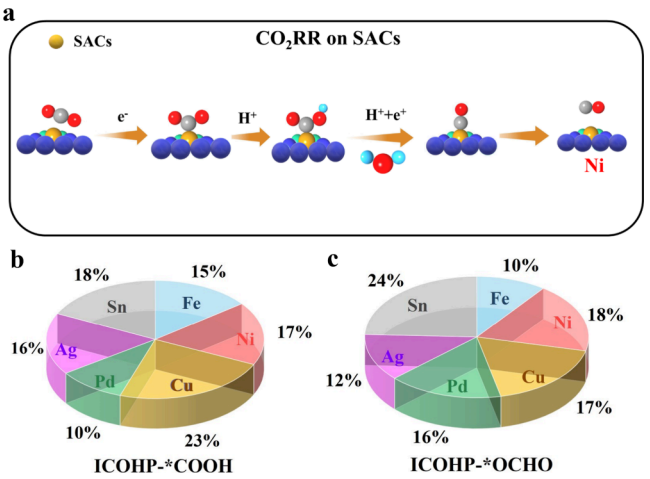

Figure 5. (a) Intermediates of *COOH and *OCHO at CO_2RR. COHP analysis for different catalysts regarding intermediates of (b) *COOH and (c) *OCHO.

optimal range. Excessively strong interactions can lead to irreversible occupation of active sites, impeding the reaction pathway, while overly weak interactions are insufficient to activate the reactant molecules, making it difficult to overcome the reaction energy barrier. Thus, a moderate ICOHP value is necessary to achieve optimal adsorption.

For CO production (Figure 5b), the ICOHP values for *COOH intermediates on Fe, Ni, Cu, Pd, Ag, and Sn were 1.10, 1.30, 1.78, 0.77, 1.27, and 1.33 eV, respectively. To more intuitively compare the relative bonding strengths of different TM-C_2N catalysts toward key intermediates, we calculated the ICOHP percentage. This parameter is obtained by dividing the ICOHP value of a given catalyst by the sum of the ICOHP values of all catalysts and then multiplying by 100%. The resulting percentage directly reflects the relative contribution and ranking of each catalyst's bonding strength within the entire set. Ni-C_2N corresponds to a percentage of 17%, representing that the contribution of its bonding orbitals with *COOH accounts for 17% of the total COHP value. It is in a moderately proportionate position. These findings support the idea that intermediates such as *COOH and SACs significantly enhance catalytic activity.

For HCOOH (Figure 5c), the ICOHP values for *OCHO intermediates on Fe, Ni, Cu, Pd, Ag, and Sn were 0.17, 0.28, 0.27, 0.25, 0.19, and 0.37 eV, respectively. For the CO pathway, the key intermediate is *COOH. Calculations indicate that both the adsorption energy and ICOHP percentage of *COOH on Ni-C_2N exhibit moderate strength. This optimal bonding ensures stable formation of *COOH while preventing excessive stabilization that would hinder subsequent *CO desorption, thereby enabling the CO pathway to achieve the lowest limiting potential on Ni-C_2N. In contrast, Cu-C_2N exhibits excessively strong bonding with *COOH, which may impede its further transformation or complicate *CO desorption, consequently increasing the overpotential of the CO pathway. For the HCOOH pathway, the key intermediate is *OCHO. Notably, although the bonding strength between Ni-C_2N and *OCHO is not the strongest, it establishes a favorable balance with its bonding strength to *COOH. This "moderate-to-weak" bonding characteristic toward both *COOH and *OCHO renders Ni-$_2$N thermodynamically more selective for CO production, as CO desorption is kinetically more favorable.

Compared to other catalysts, the adsorption energies of *COOH and *OCHO demonstrate moderate interactions with Ni active sites, respectively. This optimal interaction ensures the superior performance of Ni-C_2N in CO production synthesis. The findings demonstrate that single-atom interactions in SACs effectively modulate the electronic structure, optimizing active sites for the dynamic adsorption of key reaction intermediates. Notably, SACs display moderate adsorption energies for intermediates such as *COOH and *OCHO, pivotal for their remarkable catalytic activity. The study concludes that Ni-C_2N is the most effective catalysts for both carbon monoxide production.

CONCLUSIONS

In this study, DFT calculations were employed to design TM-C_2N catalysts and evaluate their performance in the electrochemical reduction of CO_2 to CO and HCOOH. The cohesive energies of these catalysts, spanning 7.30−7.36 eV/atom, underscore their stability. The strong orbital overlap between the metal atoms and the C_2N substrate further reinforces the structural integrity of the TM-C_2N complex. CO_2 adsorption studies reveal that TM-C_2N facilitates CO_2 capture and activation, driven by the interplay between surface architecture and active TM sites. Adsorption energies for CO_2 range from −0.94 to −3.81 eV, with notable changes in O−C−O bond angles and C−O bond lengths, indicating effective activation. Gibbs free energy calculations show that the Ni-C_2N pair exhibits lower energy barriers for the *COOH and *HCOOH intermediates, while significantly inhibiting the HER. The limiting potentials of these catalysts indicate their excellent catalytic activity. Among them, Ni-C_2N is favorable for the rate-determining steps of $*CO_2 \rightarrow$*COOH and *OCHO→ *HCOOH, with U_L values of 0.30 and 0.40 V respectively, which demonstrates that Ni-C_2N has better performance in the CO reduction pathway. In addition, the COHP values between the key intermediates of CO_2 reduction and the catalyst active site reveal that moderate adsorption ensures high catalytic performance. These results underscore the potential of transition metals as cost-effective alternatives to precious metals for efficient CO_2 electrocatalysis.

ASSOCIATED CONTENT

Data Availability Statement

Data will be made available on request.

Supporting Information

The Supporting Information is available free of charge at https://pubs.acs.org/doi/10.1021/acs.jpcc.5c07261.

Computational details including atomic structure models, ab initio molecular dynamics simulation results, density of states and charge density analysis, CO_2 adsorption configurations, molecular dynamics simulation for diffusion, Gibbs free energy data, and crystal orbital Hamilton population analysis for key intermediates (PDF)

AUTHOR INFORMATION

Corresponding Authors

Lin Tao − *School of Chemical Engineering, University of Science and Technology Liaoning, Anshan 114051, China;*

https://doi.org/10.1021/acs.jpcc.5c07261
J. Phys. Chem. C XXXX, XXX, XXX−XXX

orcid.org/0000-0002-3268-7009; Email: taolin@ustl.edu.cn

Yaqiong Su − *School of Chemistry, Engineering Research Center of Energy Storage Materials and Devices of Ministry of Education, National Innovation Platform (Center) for Industry-Education Integration of Energy Storage Technology, Xi'an Jiaotong University, Xi'an 710049, China;* orcid.org/0000-0001-5581-5352; Email: yqsu1989@xjtu.edu.cn

Baigang An − *School of Chemical Engineering, University of Science and Technology Liaoning, Anshan 114051, China;* orcid.org/0000-0001-6111-8166; Email: bgan@ustl.edu.cn

Authors

Meixu Lu − *School of Chemical Engineering, University of Science and Technology Liaoning, Anshan 114051, China;* orcid.org/0009-0008-2952-2722

Yimeng Sun − *School of Chemical Engineering, University of Science and Technology Liaoning, Anshan 114051, China*

Davoud Dastan − *Department of Materials Science and Engineering, Cornell University, Ithaca, New York 14850, United States;* orcid.org/0000-0002-4124-5763

Javed Rehman − *State Key Laboratory of Metastable Materials Science and Technology, Yanshan University, Qinhuangdao 066004, China*

Han Zhang − *School of Chemical Engineering, University of Science and Technology Liaoning, Anshan 114051, China;* orcid.org/0000-0001-6905-0952

Hongwei Zhao − *School of Chemical Engineering, University of Science and Technology Liaoning, Anshan 114051, China*

Lixiang Li − *School of Chemical Engineering, University of Science and Technology Liaoning, Anshan 114051, China*

Complete contact information is available at: https://pubs.acs.org/10.1021/acs.jpcc.5c07261

Author Contributions

Meixu Lu: data curation, formal analysis, investigation, methodology, and writing—original draft. Lin Tao: validation, data curation, methodology, supervision, funding acquisition, conceptualization, and writing—review and editing. Yaqiong Su: methodology, formal analysis, conceptualization, and writing—review and editing. Yimeng Sun: investigation, methodology, and formal analysis. Davoud Dastan: investigation, methodology, and formal analysis. Javed Rehman: investigation, methodology, and formal analysis. Han Zhang: methodology, formal analysis, and software. Hongwei Zhao: methodology, formal analysis, and software. Lixiang Li: methodology, supervision, and resources. Baigang An: supervision, formal analysis, and writing—review and editing.

Notes

The authors declare no competing financial interest.

■ ACKNOWLEDGMENTS

The funding from the National Natural Science Foundation of China (Grant Nos. 52304330 and 52371224), the Natural Science Foundation of Liaoning Province (Grant No. 2024-BS-218), the University of Science and Technology Liaoning Talent Project Grants (Grant No. 6003000317), the Outstanding Youth Fund of University of Science and Technology Liaoning (Grant No. 2023YQ11), and the Youth Fund of the Education Department of Liaoning Province (Grant No. LJKQZ20222324) are gratefully acknowledged.

■ REFERENCES

(1) Shen, S.; Guo, Q.; Wu, T.; Su, Y. The dynamic behaviors of heterogeneous interfaces in electrocatalytic CO2 reduction. *Chinese Journal of Catalysis* **2023**, *53*, 52−71.

(2) Wang, J.; Zheng, M.; Zhao, X.; Fan, W. Structure-Performance Descriptors and the Role of the Axial Oxygen Atom on M−N4−C Single-Atom Catalysts for Electrochemical CO2 Reduction. *ACS Catal.* **2022**, *12*, 5441−5454.

(3) Raju, R. K.; Rodriguez, P.; Brothers, E. N. Electrocatalytic reduction of CO2 on size-selected nanoclusters of first-row transition metal nanoclusters: a comprehensive mechanistic investigation. *Phys. Chem. Chem. Phys.* **2023**, *25*, 11630−11652.

(4) Tao, L.; Dastan, D.; Wang, W.; Poldorn, P.; Meng, X.; Wu, M.; Zhao, H.; Zhang, H.; Li, L.; An, B. Metal-Decorated InN Monolayer Senses N2 against CO2. *ACS Appl. Mater. Interfaces* **2023**, *15*, 12534−12544.

(5) Qin, Y.; Zhao, W.; Xia, C.; Yu, L.; Song, F.; Zhang, J.; Wu, T.; Cao, R.; Ding, S.; Xia, B. Y.; Su, Y. CO Intermediate-Assisted Dynamic Cu Sintering During Electrocatalytic CO(2) Reduction on Cu-N-C Catalysts. *Angew. Chem.* **2024**, *63*, No. e202404763.

(6) Pu, M.; Guo, W.; Guo, Y. Non-Noble Metal Incorporated Transition Metal Dichalcogenide Monolayers for Electrochemical CO(2) Reduction: A First-Principles Study. *ACS Appl. Mater. Interfaces* **2023**, *15*, 58388−58396.

(7) Yu, L.; Li, F.; Huang, J.; Sumpter, B. G.; Mustain, W. E.; Chen, Z. Double-Atom Catalysts Featuring Inverse Sandwich Structure for CO2 Reduction Reaction: A Synergetic First-Principles and Machine Learning Investigation. *ACS Catal.* **2023**, *13*, 9616−9628.

(8) Liu, L.; Xiao, H. Inverted Region in Electrochemical Reduction of CO(2) Induced by Potential-Dependent Pauli Repulsion. *J. Am. Chem. Soc.* **2023**, *145*, 14267−14275.

(9) Sun, Y.; Tao, L.; Wu, M.; Dastan, D.; Rehman, J.; Li, L.; An, B. Multi-atomic loaded C2N1 catalysts for CO2 reduction to CO or formic acid. *Nanoscale* **2024**, *16*, 9791−9801.

(10) Wang, Y.; Zhu, X.; Li, Y. Spin-Orbit Coupling-Dominated Catalytic Activity of Two-Dimensional Bismuth toward CO(2) Electroreduction: Not the Thinner the Better. *J. Phys. Chem. Lett.* **2019**, *10*, 4663−4667.

(11) Gao, P.; Kang, L.; Wen, C.; Kong, F.; Tao, L.; Dong, L.; Fan, M.; He, H.; Li, B.; Chen, Z. A Zn regulated Bi nanosheet catalyst for improving electrochemical CO2 reduction to formate over a wide potential window. *New J. Chem.* **2024**, *48*, 8135−8142.

(12) Nie, S.; Tao, L.; Yu, H.; Dastan, D.; Wang, W.; Hong, L.; Li, L.; An, B.; Su, Y. Theoretical and machine learning exploration of electronic factors governing Ni-centered CO2 reduction catalysts. *Phys. Chem. Chem. Phys.* **2025**, *27*, 21810−21823.

(13) Pedersen, P. D.; Melander, M. M.; Bligaard, T.; Vegge, T.; Honkala, K.; Hansen, H. A. Grand Canonical DFT Investigation of the CO2RR and HER Reaction Mechanisms on MoTe2 Edges. *J. Phys. Chem. C* **2023**, *127*, 18855−18864.

(14) Cui, Z.; Wong, A. J.; Janik, M. J.; Co, A. C. Negative Reaction Order for CO during CO(2) Electroreduction on Au. *J. Am. Chem. Soc.* **2024**, *146*, 23872−23880.

(15) Qiao, B.; Wang, A.; Yang, X.; Allard, L. F.; Jiang, Z.; Cui, Y.; Liu, J.; Li, J.; Zhang, T. Single-atom catalysis of CO oxidation using Pt1/FeOx. *Nature Chem.* **2011**, *3*, 634−641.

(16) Zhang, X.; Tao, L.; Dastan, D.; Zhang, H.; Gao, B. Tuning the electrochemical stability of carbon based single-atom structures via doping: trade-off between electrosorption/leaching behavior. *Journal of Materials Chemistry A* **2025**, *13*, 23715−23723.

(17) Zhu, W.; Xu, N.; Lin, X.; Hu, S.; Tang, S.; Shah, S. A.; Zhao, Z.; Zhang, Y.; Lu, S.; Lu, X.; Wan, J.; Xu, W.; Zhou, H.; Hu, K.; Han, Z.-K.; Wu, Y.; Song, F. Highly Selective Dual-Atom Pd Heterogeneous Catalyst Prepared by Size-Selected Cluster Beam. *ACS Catal.* **2024**, *14*, 12982−12990.

(18) Wu, S. M.; Wu, L.; Denisov, N.; Badura, Z.; Zoppellaro, G.; Yang, X. Y.; Schmuki, P. Pt Single Atoms on TiO(2) Can Catalyze Water Oxidation in Photoelectrochemical Experiments. *J. Am. Chem. Soc.* **2024**, *146*, 16363−16368.
(19) Peng, Q.; Rehman, J.; Butt, M. K.; Wang, D.; Tao, L.; Tighezza, A. M.; Dai, J. Theoretical evaluation of newly predicted VC4 monolayer for Li-ion batteries. *Journal of Energy Storage* **2024**, *95*, No. 112591.
(20) Gu, M.; Tao, L.; Dastan, D.; Dang, J.; Zhang, X.; Li, L.; An, B. Metal-enhanced carbon-nitrogen material for selective detection of hazardous gases: Insights from interface electronic states. *Surfaces and Interfaces* **2024**, *53*, No. 105097.
(21) Gu, M.; Tao, L.; Dastan, D.; Dang, J.; Fang, T.; An, B. Metal-Modified C3N1Monolayer Sensors for Battery Instability Monitoring. *Journal of Materials Chemistry A* **2024**, *12*, 15254−15264.
(22) Zhang, S.; Tao, L.; Zhang, H.; Zhao, H.; Di, F.; Li, L.; An, B. Theoretical study of metal-doped WSe2 sensors for NO detection in human exhalation. *Surfaces and Interfaces* **2025**, *73*, No. 107553.
(23) Song, C.; Tao, L.; Dang, J.; Dastan, D.; Wang, W.; Zhang, X.; Li, L.; An, B. Tuning NO2 selectivity in MoSe2 sensors via metal modification: Fermi-level electronic state control. *Computational and Theoretical Chemistry* **2025**, *1250*, No. 115296.
(24) Chen, Z.; Cao, S.; Li, J.; Yang, C.; Wei, S.; Liu, S.; Wang, Z.; Lu, X. N,S coordination in Ni single-atom catalyst promoting CO(2)RR towards HCOOH. *Phys. Chem. Chem. Phys.* **2023**, *25*, 29951−29959.
(25) Sun, P.; Liu, S.; Zheng, X.; Hu, G.; Zhang, Q.; Liu, X.; Zheng, G.; Chen, Y. Challenges and opportunities of atomic-scales reactive sites in thriving electrochemical CO2 reduction reaction. *Nano Today* **2024**, *55*, No. 102152.
(26) Ouyang, Y.; Shi, L.; Bai, X.; Ling, C.; Li, Q.; Wang, J. Selectivity of Electrochemical CO2 Reduction toward Ethanol and Ethylene: The Key Role of Surface-Active Hydrogen. *ACS Catal.* **2023**, *13*, 15448−15456.
(27) Zhang, Z.; Li, M.; Gao, R.; Yang, S.; Ma, Q.; Feng, R.; Dou, H.; Dang, J.; Wen, G.; Bai, Z.; Liu, D.; Feng, M.; Chen, Z. Selective and Scalable CO2 Electrolysis Enabled by Conductive Zinc Ion-Implanted Zeolite-Supported Cadmium Oxide Nanoclusters. *J. Am. Chem. Soc.* **2024**, *146*, 6397−6407.
(28) Wang, H.; Li, X.; Wu, J.; Zhang, D. An Experimental and Density Functional Theory Simulation Study of NO Reduction Mechanisms over Fe(0) Supported on Graphene with and without CO. *Langmuir* **2023**, *39*, 15369−15379.
(29) Wang, M.; Kong, L.; Lu, X.; Lawrence Wu, C. M. First-row transition metal embedded pyrazine-based graphynes as high-performance single atom catalysts for the CO2 reduction reaction. *J. Mater. Chem. A* **2022**, *10*, 9048−9058.
(30) Qu, G.; Wei, K.; Pan, K.; Qin, J.; Lv, J.; Li, J.; Ning, P. Emerging materials for electrochemical CO(2) reduction: progress and optimization strategies of carbon-based single-atom catalysts. *Nanoscale* **2023**, *15*, 3666−3692.
(31) Ren, Y.; Sun, X.; Qi, K.; Zhao, Z. Single atom supported on MoS2 as efficient electrocatalysts for the CO2 reduction reaction: A DFT study. *Appl. Surf. Sci.* **2022**, *602*, No. 154211.
(32) Bui, H. T. D.; Bui, V. Q.; Shao, X.; Kumar, A.; Kim, S.-G.; Le, H. M.; Kawazoe, Y.; Lee, H. Activity−Selectivity Enhancement and Catalytic Trend of CO2 Electroreduction on Metallic Dimers Supported by N-Doped Graphene: A Computational Study. *J. Phys. Chem. C* **2021**, *125*, 13176−13184.
(33) Yan, Y.; Zhao, Z.; Zhao, J.; Tang, W.; Huang, W.; Lee, J.-M. Atomic-thin hexagonal CuCo nanocrystals with d-band tuning for CO2 reduction. *Journal of Materials Chemistry A* **2021**, *9*, 7496−7502.
(34) Pan, F.; Fang, L.; Li, B.; Yang, X.; O'Carroll, T.; Li, H.; Li, T.; Wang, G.; Chen, K. J.; Wu, G. N and OH-Immobilized Cu(3) Clusters In Situ Reconstructed from Single-Metal Sites for Efficient CO(2) Electromethanation in Bicontinuous Mesochannels. *J. Am. Chem. Soc.* **2024**, *146*, 1423−1434.
(35) Dong, J.; Cheng, Y.; Li, Y.; Peng, X.; Zhang, R.; Wang, H.-T.; Wang, C.; Li, X.; Ou, P.; Pao, C.-W.; Han, L.; Pong, W.-F.; Lin, Z.; Luo, J.; Xin, H. L. Abundant (110) Facets on PdCu3 Alloy Promote Electrochemical Conversion of CO2 to CO. *ACS Appl. Mater. Interfaces* **2022**, *14*, 41969−41977.
(36) Chen, Z.; Liu, Z.; Xu, X. Accurate descriptions of molecule-surface interactions in electrocatalytic CO2 reduction on the copper surfaces. *Nat. Commun.* **2023**, *14*, 936.
(37) Wang, M.; Xiang, Y.; Lin, Y.; Sun, Y.; Zhu, Z.-z.; Wu, S.; Cao, X. p−d Orbital coupling in silicon-based dual-atom catalysts for enhanced CO2 reduction: insight into electron regulation of active center and coordination atoms. *Journal of Materials Chemistry A* **2024**, *12*, 31902−31913.
(38) Hua, Y.; Dou, B.; Lv, J.; Huang, J.; Dong, Q.; Liang, P. Understanding the mechanisms of CO2RR with Cu atom doping low Miller index surfaces in Ni metal as an effective catalyst. *J. Phys. Chem. Solids* **2026**, *208*, No. 113026.
(39) Huang, K.; Li, R.; Qi, H.; Yang, S.; An, S.; Lian, C.; Xu, Q.; Liu, H.; Hu, J. Regulating Adsorption of Intermediates via the Sulfur Modulating Dual-Atomic Sites for Boosting CO2RR. *ACS Catal.* **2024**, *14*, 8889−8898.
(40) Zaoralová, D.; Langer, R.; Otyepka, M. Iron Single-Atom Catalysts Anchored on Defect-Engineered N-Doped Graphene Reveal an Interplay between CO2 Reduction Activity and Stability. *ACS Sustainable Chem. Eng.* **2025**, *13*, 8319−8330.
(41) Chen, G.; Buraschi, M.; Al-Heidous, R.; Bonakala, S.; El-Mellouhi, F.; Cucinotta, C. S. Efficient and Selective Electrochemical CO2 to Formic Acid Conversion: A First-Principles Study of Single-Atom and Dual-Atom Catalysts on Tin Disulfide Monolayers. *J. Phys. Chem. C* **2024**, *128*, 15861−15872.
(42) Du, Y.; Chen, C. CO2 Reduction Mechanism Based on a Partially Reduced Cu Single-Atom Catalyst: A First-Principles Study. *J. Phys. Chem. C* **2025**, *129*, 6211−6224.
(43) Zhou, D.; Li, X.; Shang, H.; Qin, F.; Chen, W. Atomic regulation of metal−organic framework derived carbon-based single-atom catalysts for the electrochemical CO2 reduction reaction. *Journal of Materials Chemistry A* **2021**, *9*, 23382−23418.
(44) Jia, C.; Li, B.; Yang, J.; Jiang, S.; Gu, Z.; Sun, L.; Zhong, W.; Sharman, E.; Luo, Y.; Jiang, J. Prediction of C2N-Supported Double-Atom Catalysts with Individual/Integrated Descriptors for Electrochemical and Thermochemical CO2 Reduction. *J. Am. Chem. Soc.* **2025**, *147*, 16864−16875.
(45) Shao, Y.; Yuan, Q.; Zhou, J. Single-Atom Catalysts and Dual-Atom Catalysts for CO2 Electroreduction: Competition or Cooperation? *Small* **2023**, *19*, No. 2303446.
(46) Wu, J.; Wu, D.; Li, H.; Song, Y.; Lv, W.; Yu, X.; Ma, D. Tailoring the coordination environment of double-atom catalysts to boost electrocatalytic nitrogen reduction: a first-principles study. *Nanoscale* **2023**, *15*, 16056−16067.
(47) Umer, M.; Umer, S.; Anand, R.; Mun, J.; Zafari, M.; Lee, G.; Kim, K. S. Transition metal single atom embedded GaN monolayer surface for efficient and selective CO2 electroreduction. *Journal of Materials Chemistry A* **2022**, *10*, 24280−24289.
(48) Nitopi, S.; Bertheussen, E.; Scott, S. B.; Liu, X.; Engstfeld, A. K.; Horch, S.; Seger, B.; Stephens, I. E. L.; Chan, K.; Hahn, C.; Norskov, J. K.; Jaramillo, T. F.; Chorkendorff, I. Progress and Perspectives of Electrochemical CO2 Reduction on Copper in Aqueous Electrolyte. *Chem. Rev.* **2019**, *119*, 7610−7672.
(49) Delley, B. From molecules to solids with the DMol3 approach. *J. Chem. Phys.* **2000**, *113*, 7756−7764.
(50) Chen, X.; Zhang, Y.; Hu, R.; Qing, S.; Zhang, H. DFT study of C2N-supported Ag3M (M = Cu, Pd, and Pt) clusters as potential oxygen reduction reaction catalysts. *Chem. Eng. Sci.* **2021**, *239*, No. 116642.
(51) Li, X.; Guo, T.; Zhu, L.; Ling, C.; Xue, Q.; Xing, W. Charge-modulated CO2 capture of C3N nanosheet: Insights from DFT calculations. *Chemical Engineering Journal* **2018**, *338*, 92−98.
(52) Grimme, S. Semiempirical GGA-type density functional constructed with a long-range dispersion correction. *Journal of computational chemistry* **2006**, *27*, 1787−1799.

https://doi.org/10.1021/acs.jpcc.5c07261
J. Phys. Chem. C XXXX, XXX, XXX−XXX

(53) Wang, F.; Yang, J.; Li, J.; Han, Y.; Li, A.; Xu, R.; Feng, X.; Wang, T.; Tong, C.; Li, J.; Wei, Z. Which is Best for ORR: Single Atoms, Nanoclusters, or Coexistence? *ACS Energy Letters* **2024**, *9*, 93−101.
(54) Mathew, K.; Sundararaman, R.; Letchworth-Weaver, K.; Arias, T. A.; Hennig, R. G. Implicit solvation model for density-functional study of nanocrystal surfaces and reaction pathways. *J. Chem. Phys.* **2014**, *140*, No. 084106.
(55) Wang, M.; Ma, W.; Tan, C.; Qiu, Z.; Hu, L.; Lv, X.; Li, Q.; Dang, J. Designing Efficient Non-Precious Metal Electrocatalysts for High-Performance Hydrogen Production: A Comprehensive Evaluation Strategy. *Small* **2023**, *20*, No. e2306631.
(56) He, Y.; Li, J.; Tao, L.; Nie, S.; Fang, T.; Yin, X.; Wang, Q. First-principles calculations on the resistance and electronic properties of H2 adsorption on a CoO-SnO2 heterojunction surface. *Phys. Chem. Chem. Phys.* **2021**, *24*, 392−402.
(57) Lv, Z.; Ma, W.; Wang, M.; Dang, J.; Jian, K.; Liu, D.; Huang, D. Co-Constructing Interfaces of Multiheterostructure on MXene (Ti3C2Tx)-Modified 3D Self-Supporting Electrode for Ultraefficient Electrocatalytic HER in Alkaline Media. *Adv. Funct. Mater.* **2021**, *31*, No. 2102576.
(58) Vijay, S.; Ju, W.; Brückner, S.; Tsang, S.-C.; Strasser, P.; Chan, K. Unified mechanistic understanding of CO2 reduction to CO on transition metal and single atom catalysts. *Nature Catalysis* **2021**, *4*, 1024−1031.
(59) Christensen, O.; Bagger, A.; Rossmeisl, J. The Missing Link for Electrochemical CO2 Reduction: Classification of CO vs HCOOH Selectivity via PCA, Reaction Pathways, and Coverage Analysis. *ACS Catal.* **2024**, *14*, 2151−2161.
(60) He, Y.; Tao, L.; Li, J.; Wu, M.; Poldorn, P.; Dastan, D.; Abbasi, S.; Nie, S.; Yin, X.; Wang, Q. Atomic-level insights into selective adsorption of H2 and CO on SnO2/CoO heterojunctions. *Materials Today Nano* **2023**, *22*, No. 100334.
(61) Tao, L.; Huang, J.; Dastan, D.; Wang, T.; Li, J.; Yin, X.; Wang, Q. CO2 capture and separation on charge-modulated calcite. *Appl. Surf. Sci.* **2020**, *530*, No. 147265.
(62) Sun, X.; Li, X.; Huang, H.; Lu, W.; Xu, X.; Cui, X.; Li, L.; Zou, X.; Zheng, W.; Zhao, X. Fine Engineering of d-Orbital Vacancies of ZnN(4) via High-Shell Metal and Nonmetal Single-Atoms for Efficient and Poisoning-Resistant ORR. *Nano Lett.* **2024**, *24*, 14602−14609.
(63) Zhou, S.; Wang, M.; Wang, J.; Xin, H.; Liu, S.; Wang, Z.; Wei, S.; Lu, X. Carbon phosphides: promising electric field controllable nanoporous materials for CO2 capture and separation. *Journal of Materials Chemistry A* **2020**, *8*, 9970−9980.
(64) Nie, J.; Shi, J.; Li, L.; Xie, M.; Ouyang, Z.; Xian, M.; Huang, G.; Wan, H.; Hu, W.; Huang, W. Dense Crystalline-Amorphous Nano-Interfaces Derived from Local Reconstruction for Alkaline Hydrogen Evolution. *Adv. Energy Mater.* **2024**, *15*, No. 2404246.

https://doi.org/10.1021/acs.jpcc.5c07261
J. Phys. Chem. C XXXX, XXX, XXX−XXX